Available online at www.sciencedirect.com
ScienceDirect
Journal of Power Sources 165 (2007) 854–860
JOURNAL OF POWER SOURCES
www.elsevier.com/locate/jpowsour

# Water-gas shift reaction over magnesia-modified $Pt/CeO_2$ catalysts

Andréa M. Duarte de Farias, Ana P.M.G. Barandas, Rafael F. Perez, Marco A. Fraga *

*Laboratório de Catálise, Instituto Nacional de Tecnologia, Av. Venezuela, 82/518 20081-312 Rio de Janeiro, RJ, Brazil*

Received 14 November 2006; received in revised form 19 December 2006; accepted 20 December 2006
Available online 5 January 2007

**Abstract**

Fuel cells have risen as a clean technology for power generation and much effort has been done for converting renewable feedstock in hydrogen. The water-gas shift reaction (WGS) can be applied aiming at reducing the CO concentration in the reformate. As $Pt/CeO_2$ catalysts have been pointed out as an alternative to the industrial WGS catalysts, the modification of such systems with magnesium was investigated in this work. It was shown that the addition of MgO to $Pt/CeO_2$ increased the activity and stability of the catalyst irrespective of the preparation method used, either impregnation or co-precipitation. Based on TPR and IR spectroscopy experiments, it was seen that the presence of magnesium improved ceria reduction favoring the creation of OH groups, which are considered the active sites for the WGS reaction. The evolution of the surface species formed under reaction conditions (CO, $H_2O$, $H_2$) observed by DRIFTS evidenced that the formation of formate species and the generation of $CO_2$ is closely attached to each other; under a reaction stream containing hydrogen the presence of formate species showed to be more relevant while the $CO_2$ formation was hindered. It is suggested that the addition of MgO favors the formate decomposition and lower the carbonate concentration on the catalyst surface during WGS reaction.


*Keywords:* WGS; Fuel cell; Mg; $Pt/CeO_2$; DRIFTS

## 1. Introduction

Power generation by means of proton exchange membrane (PEM) fuel cells fed with hydrogen is a promising alternative to the internal combustion engine. However, in order to ensure long and efficient use of the cell membrane, highly pure hydrogen must be provided.

The reforming of different feedstocks, such as hydrocarbons, gasoline, methanol and ethanol may be used to generate hydrogen. These processes, irrespective of the technology route used, normally produce a mixture of CO, $CO_2$, $H_2$ and $CH_4$. The removal of CO from the reformate is compulsory, though, as it poisons the platinum-alloy catalysts found in the cell electrodes.

Water-gas shift (WGS) reaction has found then a renewed interest. It can reduce the CO content to 1 vol.%, producing an additional mole of hydrogen (Eq. (1)):

$$CO + H_2O \leftrightarrow H_2 + CO_2 \quad (\Delta H = -41.2\,\mathrm{kJ\,mol^{-1}}) \qquad (1)$$

The reformate purification must be followed by a second stage, which may be the preferential oxidation of CO (PROX) or the methanation, since it is mandatory to reach a CO level lower than 50 ppm.

The WGS reaction is well established in large steady-state operations such as hydrogen or ammonia plants. It is industrially catalyzed by two different materials depending on the temperature adopted; high temperature shift (350–450 °C) on FeCr-based catalysts and low temperature shift (180–250 °C) on CuZn-based systems. Cu-based catalysts have strong drawbacks concerning their pyrophoricity and the need for a long-term activation step, which make them inappropriate for fuel cells, especially regarding their operational cycles.

The low temperature WGS reaction is limited by kinetics and, therefore, the development of advanced catalysts has been highly demanded. Noble metal/reducible oxide systems have advantages not shown by the traditional catalysts as they can combine high activity and stability [1]. Several metal/support associations have been studied [2–4] and, consequently, kinetic [5] and mechanistic [6–9] issues have been continuously studied. Among those systems $Pt/CeO_2$ catalyst seems to be the most promising so far, exhibiting good performance.

* Corresponding author. Tel.: +55 21 21231152; fax: +55 21 21231166.
*E-mail address:* marcofra@int.gov.br (M.A. Fraga).

0378-7753/$ – see front matter © 2007 Elsevier B.V. All rights reserved.
doi:10.1016/j.jpowsour.2006.12.054

One of the proposed mechanisms is the ceria-mediated redox process [9–11], whereby CO adsorbed onto the metal is oxidized by ceria. The second step in the mechanism would involve ceria reoxidation by water as shown in the reaction scheme ($x$ is a general adsorption site):

$$CO + x \rightarrow CO_{ad}$$

$$H_2O + x \rightarrow O_{ad} + H_2$$

$$CO_{ad} + O_{ad} \rightarrow CO_2 + 2x$$

Another explanation that may describe the WGS reaction of metal promoted $CeO_2$ is the formate mechanism [6]. In this case, surface formates, produced from CO reaction with active OH groups on the partially reduced surface of ceria, could serve as intermediates, such surface formates would be decomposed to hydrogen and unidentate carbonate, prior to the liberation of $CO_2$ [6,7,12]:

$$CO + x \rightarrow CO_{ad}$$

$$H_2O + 2x \rightarrow H_{ad} + OH_{ad}$$

$$OH_{ad} + CO_{ad} \rightarrow HCOO_{ad} + x$$

$$HCOO_{ad} + x \rightarrow [CO_2]_{ad} + H_{ad}$$

$$2H_{ad} \rightarrow H_2 + 2x$$

Evidence for this mechanism was primarily obtained by infrared spectroscopy investigations and was also supported by earlier studies regarding the decomposition of formic acid over different oxides, particularly MgO, ZnO, $Fe_3O_4$ and $Cr_2O_3$ [6,13].

Even though the WGS reaction mechanism must be better understood, it is also rather important to search for stability. Deactivation of noble metal catalysts has been reported by several research groups [8,14,15] and it is definitely a relevant issue that cannot be forgotten. Amongst the several proposals to explain such process, the over-reduction of ceria due to the presence of hydrogen in the gas stream [16] and the formation of carbonate species onto the catalyst surface [14] can be outlined.

Moreover, the possibility of methane formation from hydrogen and CO in the reformate [3,17], which would decrease the $H_2$/CO ratio, is another question that must be verified when designing new catalysts for hydrogen purification by WGS. A recent report [18] has shown that the addition of basic oxides to $Pt/Al_2O_3$, which favors methanation under water-gas shift reaction conditions, hinders the hydrocarbon formation and also increases the water-gas shift reaction rate.

In this context, this contribution aims at evaluating the effects brought about by adding magnesium to $Pt/CeO_2$ concerning, especially, the catalytic activity. MgO was chosen due to its basic character and the performance in formic acid dehydrogenation.

## 2. Experimental

### 2.1. Materials preparation

Cerium oxide and magnesium oxide were synthesized by using the precipitation method described elsewhere [19]. After precipitation and washing until constant pH, the solid was calcined at 500 °C for 1 h. Two magnesia-modified supports were prepared using different methods, namely impregnation and co-precipitation.

The first sample, labeled hereinafter MgO–$CeO_2$ I, was obtained by impregnating cerium oxide with an aqueous solution of $Mg(NO_3)_2$ in which the concentration was calculated to result in the formation of a MgO monolayer. The calculation considered the oxides crystallographic data. The resulting MgO content was thus 1.4 wt.%. This solid was dried and calcined at 500 °C for 2 h with a heating rate of 10 °C $min^{-1}$.

The same precipitation procedure [19] used to prepare the bare reference oxides was followed to co-precipitate a MgO–$CeO_2$ powder (MgO–$CeO_2$ P) from their respective nitrates; the loading of MgO was the same as that used for the impregnated-prepared sample.

Finally, 1 wt.% Pt catalysts were prepared by incipient wetness impregnation with a $H_2PtCl_6$ (Merck) aqueous solution followed by calcination in air (50 mL $min^{-1}$) at 500 °C for 4 h with a heating rate of 10 °C $min^{-1}$.

### 2.2. Standard characterization

XRD patterns of all samples were conducted on a Philips X'Pert powder diffractometer with Cu Kα radiation (1.5406 Å), operating at 30 kV and 40 mA. The analyses were carried out at 0.05° per step and 2 s per step over a $2\theta$ range of 20–80°. Scherrer equation was used for crystallite mean diameter calculations based on the (1 1 1) reflection of cerium oxide.

BET specific area measurements were obtained in a Micromeritics ASAP 2010 equipment. The samples were pretreated under vacuum at 150 °C.

TPR experiments were conducted using a fixed bed tubular reactor unit equipped with a thermal conductivity detector. The gas composition was 2% $H_2/N_2$ flowed at 30mL $min^{-1}$ through 150 mg of catalyst while raising the temperature from 25 to 850 °C at a heating rate of 10 °C $min^{-1}$.

### 2.3. Diffuse reflectance infrared Fourier transform spectroscopy (DRIFTS)

The experiments were carried out in a Nicolet Magna 560 equipped with a high temperature chamber fitted with ZnSe windows (SpectraTech), which was used as the WGS reactor for in situ reaction measurements. Spectra were taken at resolution of 4 $cm^{-1}$ and 256 scans to improve the signal to noise ratio. Three different sets of experiments were performed by gradually varying the gas phase composition, basically 3 vol.% CO/He, 3 vol.% CO/10 vol.% $H_2O$/He and 60 vol.% $H_2$/3 vol.% CO/6.6 vol.% $H_2O$/He. Water was provided by using a saturator. The mixtures were first admitted into the cell at 200 °C and

spectra were collected at different temperatures after 30 min at each temperature.

### 2.4. Catalytic evaluation

The reaction was conducted with different residence times depending on the type of experiment: reaction rate calculation, which was determined under differential conditions, and long-term stability tests. The reactant mixture was primarily composed by 60.0 vol.% $H_2O$, 6.0 vol.% CO, 16.0 vol.% $H_2$, 1.6 vol.% $CO_2$ and 0.4 vol.%$CH_4$ ($N_2$ balance), simulating a typical reformate composition from partial oxidation of ethanol [20]. Shift catalysts were diluted with SiC (catalyst/SiC ratio = 1:5) and the reaction was performed at 300 °C and atmospheric pressure in a fixed bed tubular reactor attached to a TCD gas chromatograph (Agilent 6890N) equipped with a packed column Supelco (HayeSep Q) associated with a molecular sieve. Reactants flow rates and catalysts masses were varied to reach differential conditions in order to calculate reaction rates. The long-term stability tests were conducted at 300 °C, for 70 h with 400 mg of catalyst and reactant mixture flow of 30 mL $min^{-1}$. Prior to reaction, all samples were submitted to "in situ" reduction step at 350 °C for 1 h under pure hydrogen flow (30 mL $min^{-1}$).

## 3. Results and discussion

XRD patterns of the supports are shown in Fig. 1. All cerium-based materials showed only the reflections corresponding to the fluorite type structure of $CeO_2$. Basal reflections at $2\theta = 28.6°$, 33.1°, 47.5° and 56.5° are related, respectively, to the planes (1 1 1), (2 0 0), (2 2 0) and (3 1 1).

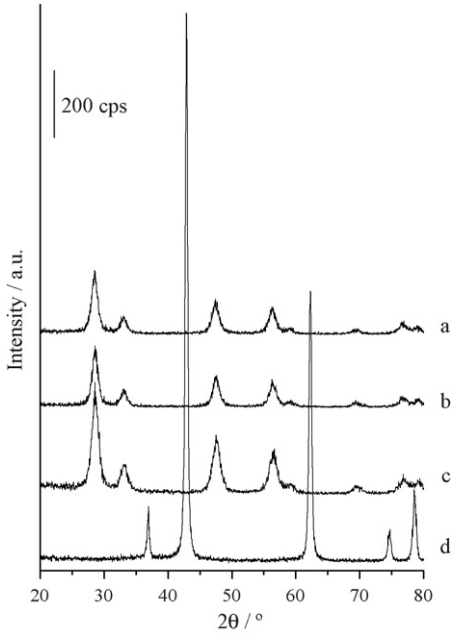


Fig. 1. XRD patterns of the supports: (a) $CeO_2$, (b) MgO–$CeO_2$ I, (c) MgO–$CeO_2$ P, and (d) MgO.

Table 1
Specific surface area and $CeO_2$ mean crystallite size of the supports

| Sample | $S_{BET}$ ($m^2\ g^{-1}$) | $d_{CeO_2}$ (nm)[a] |
|---|---|---|
| $CeO_2$ | 93 | 8.16 |
| MgO–$CeO_2$ I | 75 | 8.70 |
| MgO–$CeO_2$ P | 114 | 7.44 |
| MgO | 50 | – |

[a] Based on the (1 1 1) reflection at $2\theta = \sim 28.6°$.

The MgO XRD profile is also presented in Fig. 1d and revealed the formation of a high crystalline periclase structure [21]. It can be seen that these reflections are not present over the diffractograms of MgO–$CeO_2$ supports, suggesting that this phase is either amorphous or well dispersed onto ceria surface.

The peak broadening of cerium materials was analyzed by Scherrer equation and the results are shown in Table 1. The addition of magnesium affected the $CeO_2$ crystallite size and its influence showed to be dependent of the preparation method. The crystallite size decreased for the co-precipitated powder whereas an opposite behavior was observed over the sample prepared by impregnation. Indeed, it has been seen that co-precipitation procedure normally causes the diminishment observed for MgO–$CeO_2$ P as a consequence of the $CeO_2$ crystallization process in the presence of a second component [19,22]. On the other hand, a second calcination step applied to obtain the MgO–$CeO_2$ I is likely to be credited with the crystallite size increase.

BET surface areas are also summarized in Table 1. High specific area $CeO_2$-based materials were obtained and these results are indeed coherent with the mean crystallite size ($d_{CeO_2}$) variation resulted from the magnesium modification. It is also worth mentioning that the magnesium oxide prepared by the precipitation method described in Ref. [19] resulted in a material characterized by a specific area higher than those commonly found in the literature for such oxide (10–15 $m^2\ g^{-1}$) prepared by conventional methods [21].

It should be noted that the preparation of Pt catalysts supported on such oxides did not significantly affect their main structural and textural properties.

The reducibility of these systems was evaluated by classical hydrogen temperature-programmed reduction experiments. It is well reported in the literature that the TPR profile of bare $CeO_2$ shows basically the presence of two hydrogen consumption zones [19,23]. A first hydrogen consumption peak at low temperatures (~450 °C) is attributed to the oxide surface reduction. A second broader consumption peak is observed at higher temperatures, with a maximum at ~750 °C associated with the oxide bulk reduction. The addition of metals onto this oxide is also known to catalyze its reduction process shifting the surface reduction peak to lower temperatures [24]. This behavior is indeed shown in Fig. 2a. The peak at 360 °C is related to the reduction of both platinum and $CeO_2$ surface [25], which can be confirmed by the amount of hydrogen consumed in this stage (Table 2).

The reducibility of this system is even more affected by introducing magnesium. The TPR profiles for Pt/MgO–$CeO_2$ I and Pt/MgO–$CeO_2$ P presented also a distinct reduction peak

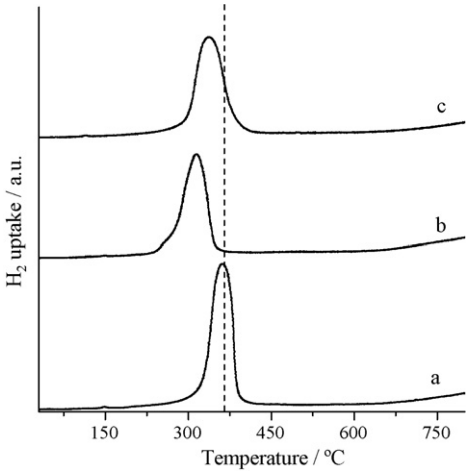


Fig. 2. TPR profiles of unmodified and Mg-modified catalysts: (a) $Pt/CeO_2$, (b) $Pt/MgO–CeO_2$ I, and (c) $Pt/CeO_2–MgO$ P.

(Fig. 2b and c), however, the position and area of this peak is pretty different for each sample. Higher hydrogen uptakes were determined for these samples (Table 2) and the reduction was centered at 315 and 336 °C for $Pt/MgO–CeO_2$ I and $Pt/MgO–CeO_2$ P, respectively, which are rather lower if compared to the $Pt/CeO_2$ catalyst. These results indicate that the catalyst reduction process is indeed facilitated by magnesium.

Taking into account the different mechanism proposals found in the literature, a series of experiments was performed by DRIFTS in order to monitor the species involved in the WGS reaction. Different gas compositions were progressively utilized in the experiments as described in the previous section.

Prior to the admission of the first mixture to the DRIFTS cell, the catalysts were reduced "in situ" under hydrogen to reproduce the reaction protocol. This reduction step was also studied by IR spectroscopy and the spectrum evolution may be seen in Fig. 3. A decrease in the intensities of absorption bands in the 1700–1250 $cm^{-1}$ range, corresponding to surface carbonate species, may be clearly seen as the temperature is raised. Simultaneously, those bands related to the stretching vibration of type II OH groups [22] are defined at around 3650 $cm^{-1}$.

After purging the cell with nitrogen, a 3 vol.% CO/He flow was then admitted at two different temperatures. The spectra resulted from this adsorption are shown in Fig. 4. Table 3 summarizes the most important band positions observed in all experiments.

The bands observed within 1800–1200 $cm^{-1}$ are related to OCO stretching vibration. This region is pretty confusing because the absorptions may be associated either to surface carbonates originated by the CO adsorption or to the formate species resulted from CO interaction with the reduced support as previously pointed out by Jacobs et al. [7]. Only by analyzing the C–H stretching vibration region (set of bands at around 2900 $cm^{-1}$), the formation of formates may be ensured.

Table 2
Catalysts hydrogen uptake from TPR experiments

| Catalyst | Reduction temperature (°C) | $H_2$ (μmol $g^{-1}$) |
|---|---|---|
| $Pt/CeO_2$ | 360 | 703 |
| $Pt/MgO–CeO_2$ I | 315 | 789 |
| $Pt/MgO–CeO_2$ P | 336 | 731 |

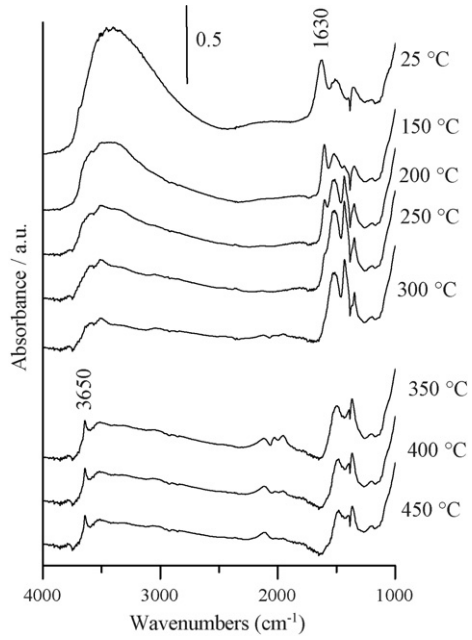


Fig. 3. DRIFTS spectra collected at different temperatures to follow the $Pt/CeO_2$ reduction under pure $H_2$.

The shoulders at around 1410 and 1350 $cm^{-1}$ may be respectively assigned to υ(OCO) asymmetric and symmetric vibrations from carbonate species. On the other hand, the bands at 1566 and 1325 $cm^{-1}$ could be attributed to the same OCO vibrations from formate species. The related C–H stretching vibrations are also seen in Fig. 4 at 2945 and 2848 $cm^{-1}$, markedly when increasing the temperature to 250 °C, confirming the generation of formate species and showing their evolution.

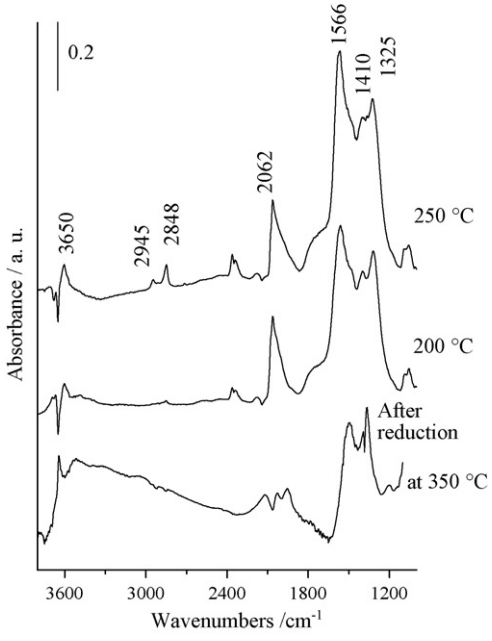


Fig. 4. DRIFTS spectra collected after CO (3 vol.% in He) adsorption at 200 and 250 °C over $Pt/CeO_2$ and after reduction at 350 °C.

Table 3
IR frequencies for the surface species analyzed

| Species | Position ($cm^{-1}$) |
|---|---|
| Pt–CO | 2062 |
| $CO_2$ | 2360, 2340 |
| OH type II | 3650 |
| Formate | |
| $\upsilon$(OCO) asymmetric | 1566 |
| $\upsilon$(OCO) symmetric | 1325 |
| $\upsilon$(C–H) | 2848, 2945 |
| Carbonate | |
| $\upsilon$(OCO) asymmetric | 1410 |
| $\upsilon$(OCO) symmetric | 1350 |

The intense peak at 2062 $cm^{-1}$ is related to linear Pt–CO vibration, indicating the presence of large platinum clusters [7]. However, the absorption tail towards lower wavenumbers might suggest that a fraction of CO adsorbs on smaller clusters of platinum. Such downshift for small particles is usually attributable to electronic effects or surface energetics [26].

Moving to the hydroxyl stretching region (3800–3600 $cm^{-1}$), type II OH groups are observed, as already mentioned. However, after CO admission the band at ~3650 $cm^{-1}$ decreases, giving rise to negative absorption bands. At this point, it is important to note that such negative bands occur because the spectra collected at 200 and 250 °C were taken by using the reduced sample spectrum (also shown in Fig. 4) as background.

Finally, $CO_2$ bands (2360 and 2340 $cm^{-1}$) can be observed as a consequence of CO oxidation.

Based on this set of bands, it can be concluded that formate species are indeed formed by the adsorption of CO onto the support reduced surface, much probably through the reaction with OH groups as suggested so far in the literature. These hydroxyl groups have been claimed to be the active sites for WGS over $Pt/CeO_2$ [7].

The second experiment was carried out by reproducing ideal reaction conditions, i.e., the spectra were collected after the adsorption of a simple $CO/H_2O$ mixture over the reduced catalyst. The same surface species as well as $CO_2$ were detected as shown in Fig. 5. Following the evolution of these bands along with temperature it may be verified that the consumption of the hydroxyl groups (Fig. 5a) occurs concomitantly to the gradual decrease of formate vibrations (Fig. 5b) while the $CO_2$ presence (Fig. 5c) becomes more significant.

By adding hydrogen to the $CO/H_2O$ mixture, in the third set of experiment, only few perturbations were observed. Fig. 6 compares only the formate C–H and the $CO_2$ regions for different gas compositions, with and without hydrogen in the stream. As could also be suggested from Fig. 5, the formation of formate species and the generation of $CO_2$ seem to be closely attached to each other; under a reaction stream containing hydrogen the presence of formate species is more relevant while the $CO_2$ formation is hindered. It is quite reasonable bearing in mind that the WGS is an equilibrium reaction (Eq. (1)) and the introduction of a product would inhibit the desired reaction.

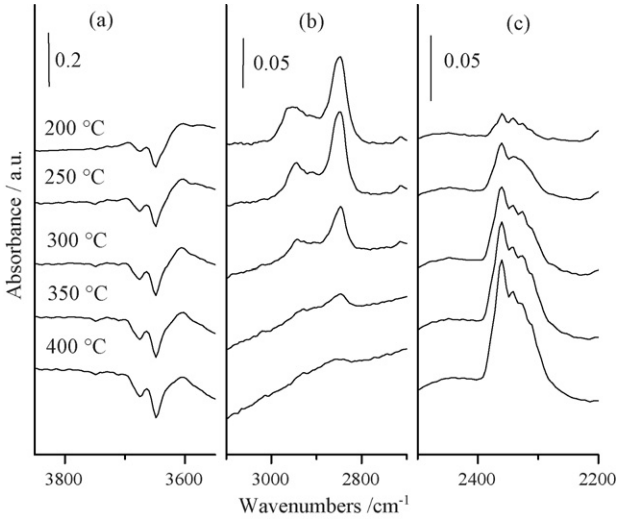


Fig. 5. DRIFTS spectra collected after adsorption of 3 vol.%CO/10 vol.%$H_2O$ over $Pt/CeO_2$: stretching vibrations bands of (a) OH, (b) C–H, and (c) $CO_2$.

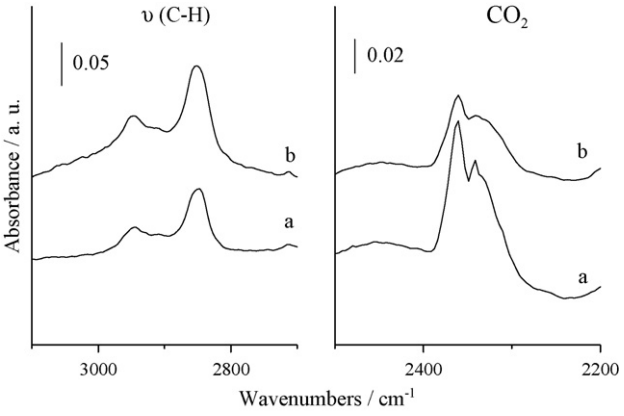


Fig. 6. Formate $\upsilon$(C–H) stretching region and $CO_2$ absorption bands after adsorption of different gas mixtures at 250 °C over $Pt/CeO_2$: (a) 3 vol.% CO/10 vol.% $H_2O$ and (b) 3 vol.% CO/6.6 vol.% $H_2O$/60.0 vol.% $H_2$.

All catalysts exhibited similar spectra with some differences in the band intensities and are not shown in detail. The results found in this work are in agreement with the formate mechanism proposed in the literature, even though the redox-based approach may not be completely ruled out. Furthermore, they evidence that the use of a gas composition as close as possible to real reaction conditions is a key factor for designing new catalytic systems.

Table 4 presents the reaction rates determined at 300 °C under differential conditions. It is shown that $CeO_2$ catalysts are in fact more active than Pt/MgO, as reported in the literature [2,27].

Table 4
Water-gas shift reaction rate at 300 °C

| Catalyst | $r$ ($\mu mol\ g^{-1}\ s^{-1}$) |
|---|---|
| $Pt/CeO_2$ | 1.89 |
| $Pt/MgO–CeO_2$ I | 2.80 |
| $Pt/MgO–CeO_2$ P | 2.63 |
| Pt/MgO | 0.71 |

Indeed, the performance of the $Pt/CeO_2$ sample prepared in this work is better than similar samples recently presented by other authors [18]. Still, it is important to note that different values for the WGS reaction rate are reported in the literature for such system, even with similar reaction conditions. Differences in the preparation procedure may be tentatively associated with such distinct performances as it deeply affects the catalyst characteristics; structural, textural, morphological and redox properties can be considered as the main factors for optimal catalyst design [2,28].

The introduction of magnesium also generated highly active catalysts (Table 4), indicating that magnesium may be playing an important role in the reaction regardless of the preparation method used for its introduction.

The calculated apparent activation energies for the $CeO_2$-based catalysts are quite similar, between 93.17 and 98.02 kJ $mol^{-1}$. It can thus be said that the reaction occurs through the same mechanism over all $CeO_2$-based catalysts studied in this work, in other words, the rate-limiting step is the same in all cases.

The DRIFTS results presented and discussed herein evidenced the presence of formate species, which could corroborate with the associative mechanism proposed in the literature. In this mechanism the reduction of the support, and consequently the generation of oxygen vacancies, is crucial as they give rise to bridging OH groups responsible for the formation of the formate species. Moreover, in such proposal, the decomposition of this species is claimed to be the key step of the reaction.

The results presented in this work suggest that the presence of MgO on $Pt/CeO_2$ catalysts would favor the formate decomposition, releasing $H_2$ and $CO_2$. Such a role played by MgO has indeed been reported for the dehydrogenation of formic acid [13,29,30]. Nevertheless, the low reaction rate observed for Pt/MgO revealed that such property is not enough by itself, and outlined the need for sites on which these formate species can be formed. Such synergism may be accomplished on $Pt/MgO–CeO_2$ systems. The TPR patterns revealed that the addition of magnesium also improved the catalysts reducibility, which should thus increase the concentration of OH active sites and, consequently, increase the concentration of surface formate species.

Catalytic stability is also a relevant issue concerning water-gas shift catalysts for fuel cell application. Hence, the Mg-modified $Pt/CeO_2$ catalysts were submitted to long-term experiments under actual reformate composition in order to briefly evaluate their overall performance (Fig. 7).

It can be observed that $Pt/CeO_2$ catalyst clearly undergoes deactivation. Right after the reaction starts up, CO conversion is around 45% and gradually decreases up to 30% after 70 h. On the contrary, the addition of magnesium significantly increases the catalyst stability. It is also worth mentioning that no methane was formed within the whole experiment over any catalyst.

The causes for the deactivation over noble metal catalysts have been still extensively debated. Amongst one of the explanations suggested so far, the formation of highly stable carbonate under reaction conditions can be mentioned [15]. Therefore, FTIR spectra in the carbonate vibration region were collected

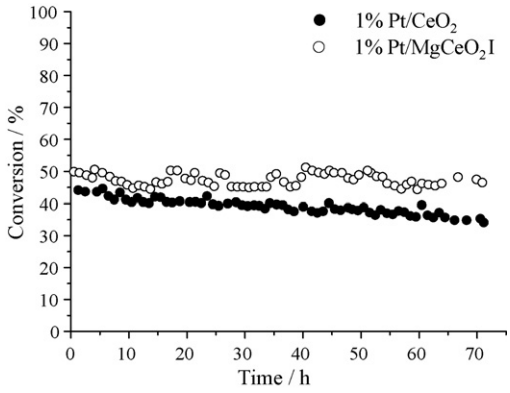


Fig. 7. Evolution of CO conversion along with reaction time under 6.0 vol.% CO, 16.0 vol.% $H_2$, 1.6 vol.% $CO_2$, 60.0 vol.% $H_2O$ and 0.4 vol.% $CH_4$ at 300 °C.

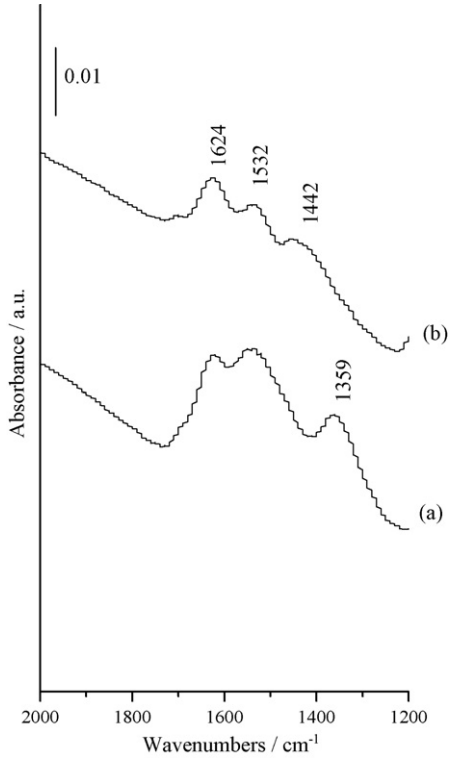


Fig. 8. FTIR spectra in the carbonate region of: (a) $Pt/CeO_2$ and (b) $Pt/MgO–CeO_2$ I.

with the catalysts after the long-term experiments and they are depicted in Fig. 8. Indeed, it may be seen that the $Pt/CeO_2$, which showed to deactivate in time, presented stronger absorptions at 1624, 1532 and 1359 $cm^{-1}$, related to different carbonate species onto the catalyst surface. Although these bands are also present on the magnesium-modified sample spectrum, their intensity is rather lower, indicating that a lower concentration of carbonate are formed over this catalyst.

## 4. Conclusions

Addition of MgO to $Pt/CeO_2$ increased the activity and stability of the catalyst. It seems to favor the formate decomposition and lower the carbonate concentration on the catalyst

surface during WGS reaction. The presence of magnesium also improved ceria reduction favoring the creation of OH groups, which are considered to be the active sites for the WGS reaction.

## Acknowledgements

The authors are indebted to Dr. Priscila Zonetti (LDPC/FEQ/UNICAMP) for her assistance in the TPR experiments. The financial support from CTENERG/FINEP (01.04.0525.00) is also acknowledged.

## References

[1] L. Mendelovici, M. Steinberg, J. Catal. 96 (1985) 285–287.
[2] P. Panagiotopoulou, D.I. Kondarides, Catal. Today 112 (2006) 49–52.
[3] C. Wheeler, A. Jhalani, E.J. Klein, S. Tummala, L.D. Schmidt, J. Catal. 223 (2004) 191–199.
[4] Q. Fu, H. Satsburg, M. Flytzani-Stephanopoulos, Science 301 (2003) 935–938.
[5] A.B. Mhadeshwar, D.G. Vlachos, Catal. Today 105 (2005) 162–172.
[6] T. Shido, A. Yamaguchi, K. Asakura, Y. Iwasawa, J. Mol. Catal. A 163 (2000) 67–83.
[7] G. Jacobs, L. Williams, U. Graham, D. Sparks, B. Davis, J. Phys. Chem. B 107 (2003) 10398–10404.
[8] R.J. Gorte, S. Zhao, Catal. Today 104 (2005) 18–24.
[9] T. Bunluesin, R.J. Gorte, G.W. Graham, Appl Catal 15 (1998) 107–114.
[10] Y. Li, Q. Fu, M. Flytzani-Stephanopoulos, Appl. Catal. B 27 (2000) 179–191.
[11] Q. Fu, A. Weber, M. Flytzani-Stephanopoulos, Catal. Lett. 77 (2001) 87–95.
[12] G. Jacobs, U.M. Graham, E. Chenu, P.M. Patterson, A. Dozier, B.H. Davis, J. Catal. 229 (2005) 499–512.
[13] T. Shido, K. Asakura, Y. Iwasawa, J. Catal. 122 (1990) 55–67.
[14] A. Goguet, F. Meunier, J.P. Breen, R. Burch, M.I. Petch, A. Faur Ghenciu, J. Catal. 226 (2004) 382–392.
[15] X. Liu, W. Ruettinger, X. Xu, R. Farrauto, Appl. Catal. B 56 (2005) 69–75.
[16] J.M. Zalc, V. Sokolovskii, D.G. Löffler, J. Catal. 206 (2002) 169–171.
[17] T. Utaka, T. Okanishi, T. Takeguchi, R. Kikuchi, K. Eguchi, Appl. Catal. A 245 (2003) 343–351.
[18] A.A. Phatak, N.A. Koryabkina, N.A. Deskins, K.T. Thomson, W.F. Ruettinger, R.J. Farrauto, F.H. Ribeiro, Proceedings of the 19th North American Catalysis Society Meeting, Philadelphia, 2005, p. 302.
[19] S. Letichevsky, C.A. Tellez, R.R. De Avillez, M.I.P. Silva, M.A. Fraga, L.G. Appel, Appl. Catal. B 58 (2005) 203–210.
[20] A.M. Silva, A.P.M.G. Barandas, L.O.O. Costa, L.E.P. Borges, L.V. Mattos, F.B. Noronha, Catal. Today, in press.
[21] M.A. Aramendia, J.A. Benitez, V. Borau, C. Jiménez, J.M. Marinas, J.R. Ruiz, F.J. Urbano, Colloids Surf. A 168 (2000) 27–33.
[22] A. Laachir, V. Perrichon, A. Badri, J. Lamotte, E. Catherine, J.-C. Lavalley, J. El Fallah, L. Hilaire, F. Le Normand, E. Quéméré, G.N. Sauvion, O. Touret, J. Chem. Soc., Faraday Trans. 87 (1991) 1601–1609.
[23] V. Perrichon, A. Laachir, G. Begere, R. Frety, L. Tournayan, O. Touret, J. Chem. Soc., Faraday Trans. 90 (1994) 1.
[24] S. Ricote, G. Jacobs, M. Milling, Y. Ji, P.M. Patterson, B.H. Davis, Appl. Catal. A 303 (2006) 35–47.
[25] L.V. Mattos, E.R. de Oliveira, P.D. Resende, F.B. Noronha, F.B. Passos, Catal. Today 77 (2002) 245–256.
[26] G. Jacobs, L. Williams, U. Graham, G.A. Thomas, D.E. Sparks, B.H. Davis, Appl. Catal. A 252 (2003) 107–118.
[27] E. Chenu, G. Jacobs, A.C. Crawford, R.A. Keogh, P.M. Patterson, D.E. Sparks, B.H. Davis, Appl. Catal. B 59 (2005) 45–56.
[28] P. Panagiotopoulou, D.I. Kondarides, J. Catal. 225 (2004) 327–336.
[29] G. Jacobs, P.M. Patterson, U. Graham, A.C. Crawford, A. Dozier, B.H. Davis, J. Catal. 235 (2005) 79–91.
[30] S. Ricote, G. Jacobs, M. Milling, Y. Ji, P.M. Patterson, B.H. Davis, Appl. Catal A 303 (2006) 35–47.